CLNS 94/1314
CLEO 94–25
December 13, 1994

First Measurement of the Rate for the Inclusive Radiative Penguin Decay $b \to s\gamma$

M.S. Alam,[1] I.J. Kim,[1] Z. Ling,[1] A.H. Mahmood,[1] J.J. O'Neill,[1] H. Severini,[1] C.R. Sun,[1] F. Wappler,[1] G. Crawford,[2] C. M. Daubenmier,[2] R. Fulton,[2] D. Fujino,[2] K.K. Gan,[2] K. Honscheid,[2] H. Kagan,[2] R. Kass,[2] J. Lee,[2] M. Sung,[2] C. White,[2] A. Wolf,[2] M.M. Zoeller,[2] F. Butler,[3] X. Fu,[3] B. Nemati,[3] W.R. Ross,[3] P. Skubic,[3] M. Wood,[3] M. Bishai,[4] J. Fast,[4] E. Gerndt,[4] J.W. Hinson,[4] R.L. McIlwain,[4] T. Miao,[4] D.H. Miller,[4] M. Modesitt,[4] D. Payne,[4] E.I. Shibata,[4] I.P.J. Shipsey,[4] P.N. Wang,[4] M. Battle,[5] J. Ernst,[5] L. Gibbons,[5] Y. Kwon,[5] S. Roberts,[5] E.H. Thorndike,[5] C.H. Wang,[5] J. Dominick,[6] M. Lambrecht,[6] S. Sanghera,[6] V. Shelkov,[6] T. Skwarnicki,[6] R. Stroynowski,[6] I. Volobouev,[6] G. Wei,[6] P. Zadorozhny,[6] M. Artuso,[7] M. Gao,[7] M. Goldberg,[7] D. He,[7] N. Horwitz,[7] G.C. Moneti,[7] R. Mountain,[7] F. Muheim,[7] Y. Mukhin,[7] S. Playfer,[7] Y. Rozen,[7] S. Stone,[7] X. Xing,[7] G. Zhu,[7] J. Bartelt,[8] S.E. Csorna,[8] Z. Egyed,[8] V. Jain,[8] D. Gibaut,[9] K. Kinoshita,[9] P. Pomianowski,[9] B. Barish,[10] M. Chadha,[10] S. Chan,[10] D.F. Cowen,[10] G. Eigen,[10] J.S. Miller,[10] C. O'Grady,[10] J. Urheim,[10] A.J. Weinstein,[10] M. Athanas,[11] W. Brower,[11] G. Masek,[11] H.P. Paar,[11] J. Gronberg,[12] C.M. Korte,[12] R. Kutschke,[12] S. Menary,[12] R.J. Morrison,[12] S. Nakanishi,[12] H.N. Nelson,[12] T.K. Nelson,[12] C. Qiao,[12] J.D. Richman,[12] A. Ryd,[12] D. Sperka,[12] H. Tajima,[12] M.S. Witherell,[12] R. Balest,[13] K. Cho,[13] W.T. Ford,[13] D.R. Johnson,[13] K. Lingel,[13] M. Lohner,[13] P. Rankin,[13] J.G. Smith,[13] J.P. Alexander,[14] C. Bebek,[14] K. Berkelman,[14] K. Bloom,[14] T.E. Browder,[14*] D.G. Cassel,[14] H.A. Cho,[14] D.M. Coffman,[14] D.S. Crowcroft,[14] P.S. Drell,[14] D.J. Dumas,[14] R. Ehrlich,[14] P. Gaidarev,[14] M. Garcia-Sciveres,[14] B. Geiser,[14] B. Gittelman,[14] S.W. Gray,[14] D.L. Hartill,[14] B.K. Heltsley,[14] S. Henderson,[14] C.D. Jones,[14] S.L. Jones,[14] J. Kandaswamy,[14] N. Katayama,[14] P.C. Kim,[14] D.L. Kreinick,[14] G.S. Ludwig,[14] J. Masui,[14] J. Mevissen,[14] N.B. Mistry,[14] C.R. Ng,[14] E. Nordberg,[14] J.R. Patterson,[14] D. Peterson,[14] D. Riley,[14] S. Salman,[14] M. Sapper,[14] F. Würthwein,[14] P. Avery,[15] A. Freyberger,[15] J. Rodriguez,[15] S. Yang,[15] J. Yelton,[15] D. Cinabro,[16] T. Liu,[16] M. Saulnier,[16] R. Wilson,[16] H. Yamamoto,[16] T. Bergfeld,[17] B.I. Eisenstein,[17] G. Gollin,[17] B. Ong,[17] M. Palmer,[17] M. Selen,[17] J. J. Thaler,[17] K.W. Edwards,[18] M. Ogg,[18] A. Bellerive,[19] D.I. Britton,[19] E.R.F. Hyatt,[19] D.B. MacFarlane,[19] P.M. Patel,[19] B. Spaan,[19] A.J. Sadoff,[20] R. Ammar,[21] P. Baringer,[21] A. Bean,[21] D. Besson,[21] D. Coppage,[21] N. Copty,[21] R. Davis,[21] N. Hancock,[21] M. Kelly,[21] S. Kotov,[21] I. Kravchenko,[21] N. Kwak,[21] H. Lam,[21] Y. Kubota,[22] M. Lattery,[22] M. Momayezi,[22] J.K. Nelson,[22] S. Patton,[22] R. Poling,[22] V. Savinov,[22] S. Schrenk,[22] and R. Wang[22]

(CLEO Collaboration)

[1]*State University of New York at Albany, Albany, New York 12222*
[2]*Ohio State University, Columbus, Ohio, 43210*
[3]*University of Oklahoma, Norman, Oklahoma 73019*
[4]*Purdue University, West Lafayette, Indiana 47907*
[5]*University of Rochester, Rochester, New York 14627*
[6]*Southern Methodist University, Dallas, Texas 75275*
[7]*Syracuse University, Syracuse, New York 13244*
[8]*Vanderbilt University, Nashville, Tennessee 37235*
[9]*Virginia Polytechnic Institute and State University, Blacksburg, Virginia, 24061*
[10]*California Institute of Technology, Pasadena, California 91125*
[11]*University of California, San Diego, La Jolla, California 92093*
[12]*University of California, Santa Barbara, California 93106*
[13]*University of Colorado, Boulder, Colorado 80309-0390*
[14]*Cornell University, Ithaca, New York 14853*
[15]*University of Florida, Gainesville, Florida 32611*
[16]*Harvard University, Cambridge, Massachusetts 02138*
[17]*University of Illinois, Champaign-Urbana, Illinois, 61801*
[18]*Carleton University, Ottawa, Ontario K1S 5B6 and the Institute of Particle Physics, Canada*
[19]*McGill University, Montréal, Québec H3A 2T8 and the Institute of Particle Physics, Canada*
[20]*Ithaca College, Ithaca, New York 14850*
[21]*University of Kansas, Lawrence, Kansas 66045*
[22]*University of Minnesota, Minneapolis, Minnesota 55455*

Abstract

We have measured the inclusive $b \to s\gamma$ branching ratio to be $(2.32 \pm 0.57 \pm 0.35) \times 10^{-4}$, where the first error is statistical and the second is systematic. Upper and lower limits on the branching ratio, each at 95% CL, are $\mathcal{B}(b \to s\gamma) < 4.2 \times 10^{-4}$ and $\mathcal{B}(b \to s\gamma) > 1.0 \times 10^{-4}$. These limits restrict the parameters of extensions of the Standard Model.

PACS numbers: 13.25Hw, 14.40.Nd

Typeset using REVTEX

*Permanent address: University of Hawaii at Manoa

The transition $b \to s\gamma$ is a flavor-changing neutral current process. It is described by a penguin diagram in which a virtual W is exchanged in a loop with a top quark, with a photon emitted from any of the lines [1]. There are large QCD corrections to the penguin diagram. Progressively more complete calculations, based on the method of renormalization-group-improved perturbation theory, have been applied to the problem [2]. There is now general agreement on the full leading-log calculation [3]. Some of the next-to-leading-logarithmic QCD corrections have been calculated [4]. The QCD corrections increase the rate by a factor of 2–3. The Standard Model branching ratio for a leading-log calculation is $(2.8 \pm 0.8) \times 10^{-4}$ [5], where the error is dominated by the uncertainty in the renormalization scale $m_b/2 < \mu < 2m_b$. If those next-to-leading log terms that have been calculated are included, the branching ratio falls to 1.9×10^{-4} [6]. The branching ratio is sensitive to the existence of a charged Higgs [7], anomalous $WW\gamma$ coupling [8], and other non-standard-model phenomena [9].

CLEO's observation [10] of the decay $B \to K^*(892)\gamma$, the first conclusive evidence for a penguin decay, established the existence of penguin diagrams generally and of $b \to s\gamma$ in particular. Since there are large theoretical uncertainties in the hadronization process, $\Gamma(B \to K^*\gamma)$ gives only a rough measure of $\Gamma(b \to s\gamma)$, the quantity of theoretical interest. Here we present a measurement of the branching ratio for the inclusive process $b \to s\gamma$. The data were taken with the CLEO detector at the Cornell Electron Storage Ring (CESR), and consist of 2.01 fb^{-1} on the $\Upsilon(4S)$ resonance and 0.96 fb^{-1} at a center-of-mass energy 60 MeV below the resonance. The on-resonance sample contains 2.15 million $B\bar{B}$ events and 6.6 million continuum events. The CLEO detector [11] measures charged particles over 95% of 4π steradians with a system of cylindrical drift chambers. Its barrel and endcap CsI electromagnetic calorimeters cover 98% of 4π. The energy resolution for photons near 2.5 GeV in the central angular region ($|\cos\theta_\gamma| < 0.7$) is 2%.

Our signature for $b \to s\gamma$ is a photon from B-meson decay with energy between 2.2 and 2.7 GeV, the Doppler-broadened line expected from motion of the b quark in a B meson and a B meson in the lab. Spectator model calculations [12] indicate that 75-90% of the signal lies in this range. Backgrounds from other B-decay processes are small and calculable. There are very large backgrounds from the continuum, both from the initial-state-radiation (ISR) process $e^+e^- \to q\bar{q}\gamma$, and from the continuum reaction $e^+e^- \to q\bar{q}$, with the high energy photon arising from the hadronic debris (π^0, η, $\omega \to \pi^0\gamma$, *etc.*). We suppress the continuum with two methods and subtract what remains using off-resonance data.

We select events that pass general hadronic event selection criteria [13]. We further require that the event contain a high energy calorimeter cluster with $|\cos\theta_\gamma| < 0.7$ and unmatched to a charged particle track. The vast majority of photons, both from continuum and $B\bar{B}$ events, are π^0 and η decay products. We discard those high energy clusters which, when paired with another γ in the event, have a $\gamma\gamma$ mass consistent with a π^0 or η. Finally, we require that the lateral energy distribution of the cluster be consistent with that of a single isolated photon, thus suppressing random overlaps, single-cluster π^0's, and non-photon clusters.

The first method [13] for suppressing continuum background uses eight carefully chosen event-shape variables: R_2, $S_\perp$, R_2', $\cos\theta'$ as defined in Ref. [10], and the energies in 20° and

30° cones, parallel and antiparallel to the high energy photon direction. We combine the eight variables into a single variable r which tends towards $+1$ for $b \to s\gamma$ and tends towards -1 for ISR and $q\bar{q}$. A neural network is used for this task. Distributions in r are shown in Fig. 1. There is substantial discrimination between signal and background, and good agreement between Monte Carlo (MC) background and off-resonance data. We perform a weighted sum of candidate high energy photon events, with an r-dependent weighting, optimized with MC samples of signal and background. This weighting procedure is equivalent to performing a 1-parameter fit to the r distribution.

In the second method for suppressing the continuum, we search each event for combinations of particles that reconstruct to a $B \to X_s\gamma$ decay. For X_s we use: $K_s^0 \to \pi^+\pi^-$ or a charged track with dE/dx consistent with a kaon; and 1–4 π's, of which one may be a π^0. There are reconstruction ambiguities and cross-feed between decay modes, but these are not important because this method is used only to suppress background and *not* for a mode-by-mode B-reconstruction analysis. In each event, we pick the combination that minimizes an overall χ^2, which includes χ_B^2 (see below), together with contributions from dE/dx and K_s^0 and π^0 mass deviations, where relevant. We calculate the beam-constrained mass M_B and energy E_B of the combination, and also $\cos\theta_{tt}$, where θ_{tt} is the angle between the thrust axis of the candidate B and the thrust axis of the rest of the event. We discriminate between signal and background by requiring $|\cos\theta_{tt}| < 0.6$ and $\chi_B^2 < 6.0$, where

$$\chi_B^2 = \left(\frac{M_B - 5.279}{\sigma_M}\right)^2 + \left(\frac{E_B - E_{beam}}{\sigma_E}\right)^2. \tag{1}$$

The two methods for suppressing the continuum are complementary. The B-reconstruction method has lower efficiency for $b \to s\gamma$ (9% vs 32%) but a factor of 4 better signal-to-noise, so the two methods have nearly equal sensitivity, and are only slightly correlated.

There are backgrounds from B decay processes other than $b \to s\gamma$, in particular from $b \to cW^-$, $b \to uW^-$, and $b \to sg$. As a first approximation, we take these from MC. We then correct for any difference between the π^0 momentum spectra from data and MC, and similarly for the η momentum spectra. Thus these backgrounds are determined from data. It is only for those small B-decay backgrounds *not* from π^0 or η that we rely on MC.

The photon energy spectra from the event-shape and B-reconstruction analyses are shown in Figs. 2 and 3, respectively. In both cases, the on-resonance yield exceeds the background in the energy interval $2.2 - 2.7$ GeV, demonstrating the presence of $b \to s\gamma$. A signal of the expected shape is evident in the subtracted spectra [14]. Yields between 2.2 and 2.7 GeV are given in Table 1.

The B-reconstruction technique selects a "best" X_s candidate for $B \to X_s\gamma$, thus providing an "apparent X_s mass spectrum" (Fig. 4). Although reconstruction ambiguities and cross-feed must be taken into account before quantitative use can be made of it, there is clear evidence both for $B \to K^*(892)\gamma$ and for X_s systems in the 1-2 GeV range. The rate for $K^*(892)\gamma$ extracted by a fit to the distribution in Fig. 4 is consistent with our previous measurement[10].

To calculate detection efficiencies, we model the particle content of X_s in $b \to s\gamma$ with conventional models of quark hadronization [13]. We model the X_s mass distribution with the spectator model of Ali and Greub [12], which includes gluon bremsstrahlung and higher-order radiative effects. In the Ali-Greub model, we vary the Fermi-momentum parameter P_F and spectator-quark mass simultaneously so that the b-quark average mass $\langle m_b \rangle$ is constant at 4.87 ± 0.10 GeV, a value suggested by recent theoretical work [15]. We take $P_F = 270 \pm 40$ MeV/c, based on fits to CLEO $B \to X\ell\nu$ data with the same $\langle m_b \rangle$.

We find $\mathcal{B}(b \to s\gamma) = (1.88 \pm 0.74) \times 10^{-4}$ with the event-shape analysis, and $(2.75 \pm 0.67) \times 10^{-4}$ with the B-reconstruction analysis (statistical errors only). Allowing for correlations, the difference is 1.1 standard deviation. We combine the two results, allowing for correlations, obtaining $\mathcal{B}(b \to s\gamma) = (2.32 \pm 0.57 \pm 0.35) \times 10^{-4}$, where the first error is statistical and the second is systematic (including model dependence). We find $\mathcal{B}(b \to s\gamma) < 4.2 \times 10^{-4}$, $\mathcal{B}(b \to s\gamma) > 1.0 \times 10^{-4}$, each limit at 95% CL.

Uncertainties in yield and efficiency comprise the systematic error in $\mathcal{B}(b \to s\gamma)$. In units of 10^{-4}, these contributions (labeled by source of uncertainty) are: $\pm$ 0.03 (On-Off luminosity ratio [16]), $\pm$ 0.08 (π^0 veto efficiency), $\pm$0.10 (On-Off energy difference correction), $\pm$ 0.08 ($B^+B^-/B^0\bar{B}^0$ production ratio), $\pm$ 0.23 ($\langle m_b \rangle$), $\pm$ 0.002 (P_F), $\pm$ 0.12 (particle content of X_s), $\pm$ 0.16 (MC modeling).

Our measurement is in good agreement with the Standard Model expectation. We illustrate the implications for non-standard models with two examples [17]. A charged Higgs with Model II coupling would increase the $b \to s\gamma$ branching ratio [7], so our upper limit on $b \to s\gamma$ provides a lower limit on charged Higgs mass: $M_{H^\pm} > \{244 + 63/(\tan\beta)^{1.3}\}$ GeV, where $\tan\beta = v_2/v_1$, the ratio of vacuum expectation values for the two doublets. With additional non-standard-model effects this limit can be circumvented. For example, in SUSY, if chargino and scalar top are light, their contribution can cancel the charged Higgs contribution [18].

Anomalous $WW\gamma$ couplings could either increase or decrease the $b \to s\gamma$ branching ratio [8], so both our upper and lower limits rule out portions of the $\Delta\kappa - \lambda$ space that describes these anomalous couplings (Fig. 5). Also shown in Fig. 5 are the regions allowed and excluded by $\bar{p}p \to W\gamma X$ measurements [19]. The two types of measurements are complementary.

In summary, the inclusive branching ratio for $b \to s\gamma$ has been determined using two analysis methods yielding consistent results. Our measurement is in good agreement with Standard Model predictions, and places constraints on other models. These constraints will improve with completion of a next-to-leading-log calculation.

We gratefully acknowledge the effort of the CESR staff in providing us with excellent luminosity and running conditions. We thank A. Ali and C. Greub for performing spectator model calculations for us. J. Hewett and T. Rizzo have helped us understand the implications of $b \to s\gamma$ for non-standard models. This work was supported by the National Science Foundation, the U.S. Dept. of Energy, the Heisenberg Foundation, the Alexander von Humboldt Stiftung, the SSC Fellowship program of TNRLC, Natural Sciences and Engineering Research Council of Canada, and the A.P. Sloan Foundation.

REFERENCES

[1] B. Campbell and P. O'Donnell, Phys. Rev. D **25**, 1989 (1982).

[2] S. Bertolini *et al.*, Phys. Rev. Lett. **59**, 180 (1987); N. Deshpande *et al.*, Phys. Rev. Lett. **59**, 183 (1987); B. Grinstein *et al.*, Phys. Lett. B **202**,138 (1988); R. Grigjanis *et al.*, Phys. Lett. B **213**, 335 (1988); G. Cella *et al.*, Phys. Lett. B **248**, 181 (1990); M. Misiak, Phys. Lett. B **269**, 161 (1991).

[3] M. Ciuchini *et al.*, Phys. Lett. B **316**, 127 (1993); M. Misiak, Phys. Lett. B **321**, 113 (1994); G. Cella *et al.*, Phys. Lett. B **325**, 227 (1994).

[4] A. Ali and C. Greub, Phys. Lett. B **259**, 182 (1991); Z. Phys. C **60**, 433 (1993); A. Buras *et al.*, Nucl. Phys. **B370**, 69 (1992); **B375**, 501 (1992); **B400**, 37 (1993); 75 (1993); M. Ciuchini *et al.*, Phys. Lett. B **301**, 263 (1993); Nucl. Phys. **B415**, 403 (1994).

[5] A. Buras *et al.*, Nucl. Phys. **B424**, 374 (1994).

[6] M. Ciuchini *et al.*, Phys. Lett. B **334**, 137 (1994).

[7] R. Ellis *et al.*, Phys. Lett. B **179**, 119 (1986); T. Rizzo, Phys Rev. D **38**, 820 (1988); B. Grinstein and M. Wise, Phys. Lett. B **201**, 274 (1988); W. Hou and R. Wiley, Phys Lett. B **202**, 591 (1988); C. Geng and J. Ng, Phys Rev. D **38**, 2858 (1988); V. Barger, J. Hewett, and R. Phillips, Phys. Rev. D **41**, 3421 (1990).

[8] S. Chia, Phys. Lett. B **240**, 465 (1990); K. Peterson, Phys. Lett. B **282**, 207 (1992); T. Rizzo, Phys. Lett. B **315**, 471 (1993); U. Baur, in Proceedings of the *Summer Workshop on B Physics*, Snowmass, CO, 1993; X. He and B. McKellar, Phys. Lett. B **320**, 165 (1994).

[9] For a review of implications of $b \to s\gamma$ for non-standard models, see J. Hewett, SLAC-PUB-6521 (1994).

[10] R. Ammar *et al.* (CLEO), Phys. Rev. Lett. **71**, 674 (1993).

[11] Y. Kubota *et al.* (CLEO), Nucl. Instrum. Meth. A **320**, 66 (1992).

[12] A. Ali and C. Greub, Phys. Lett. B **259**, 182 (1991).

[13] J.A. Ernst, Ph.D. thesis, Univ. of Rochester (1995).

[14] The fit of the MC prediction to the data in Fig. 2(b) has a χ^2 of 5.8 for 7 degrees of freedom. We have searched for explanations of the high point at 3.0–3.5 GeV, and found none (other than statistical fluctuation).

[15] M. Voloshin and Y. Zaitsev, Sov. Phys. Usp. **30**, 553 (1987); C. Davies *et al.*, Phys. Rev. Lett. **73**, 2654 (1994).

[16] G. Crawford *et al.* (CLEO), Nucl. Instrum. Meth. A **345**, 429 (1994).

[17] We use $m_t = 175$ GeV, leading-log terms only, and $m_b/2 < \mu < 2m_b$. We assume a 10% theoretical uncertainty in addition to the renormalization scale uncertainty.

[18] S. Bertolini *et al.*, Nucl. Phys. **B294**, 321 (1987); **B353**, 591 (1991); Y. Okada, Phys. Lett. B **315**, 119 (1993); R. Garisto and J.N. Ng, Phys. Lett. B **315**, 372 (1993).

[19] F. Abe *et al.* (CDF), Fermilab-Pub-94/236-E; J. Ellison (D0), Proceedings of 1994 Meeting of Division of Particles and Fields, Albuquerque, NM (1994).

FIGURES

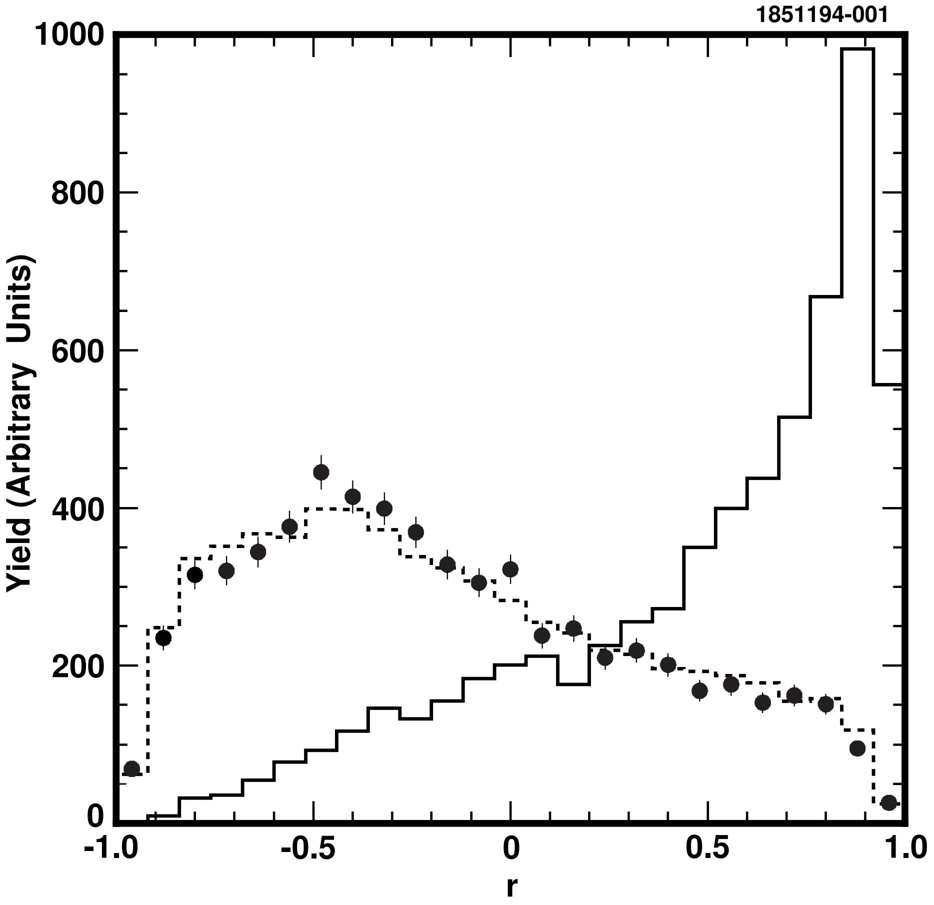

FIG. 1. Distributions in the neural net variable r, for Monte Carlo samples of $b \to s\gamma$ signal (solid histogram) and continuum background (dashed histogram), and for the off-resonance data sample (points).

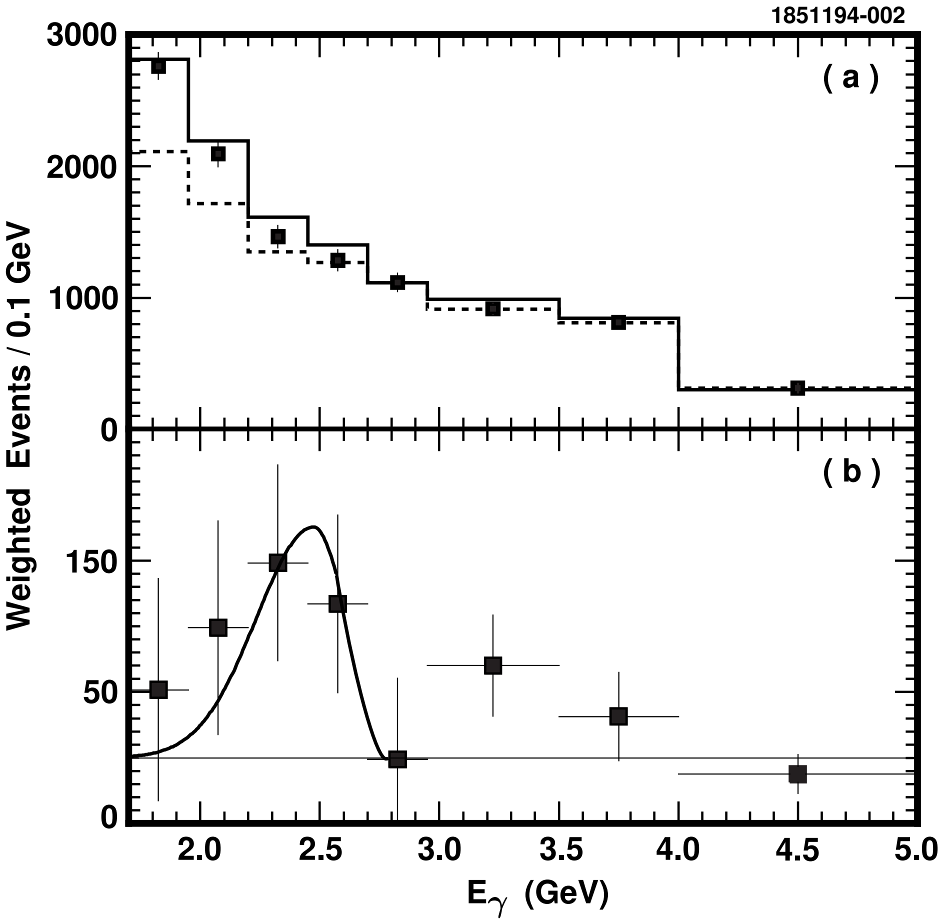

FIG. 2. Photon energy spectra from the event-shape analysis. (a) On-resonance (solid histogram), scaled off-resonance (dashed histogram), and sum of off-resonance and background from $\Upsilon(4S)$ (squares). (b) Background-subtracted data (points) and Monte Carlo prediction for the shape of the $b \to s\gamma$ signal (solid curve)[14].

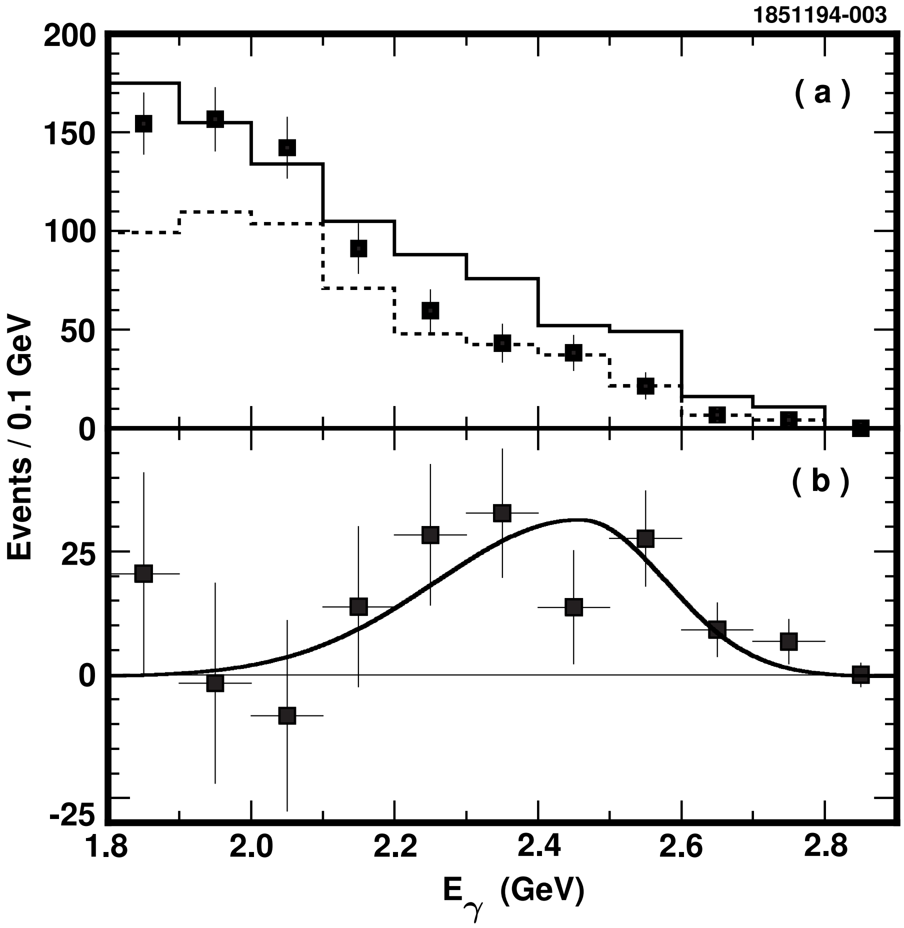

FIG. 3. Photon energy spectra from the B-reconstruction analysis. Symbols are defined as in Fig. 2.

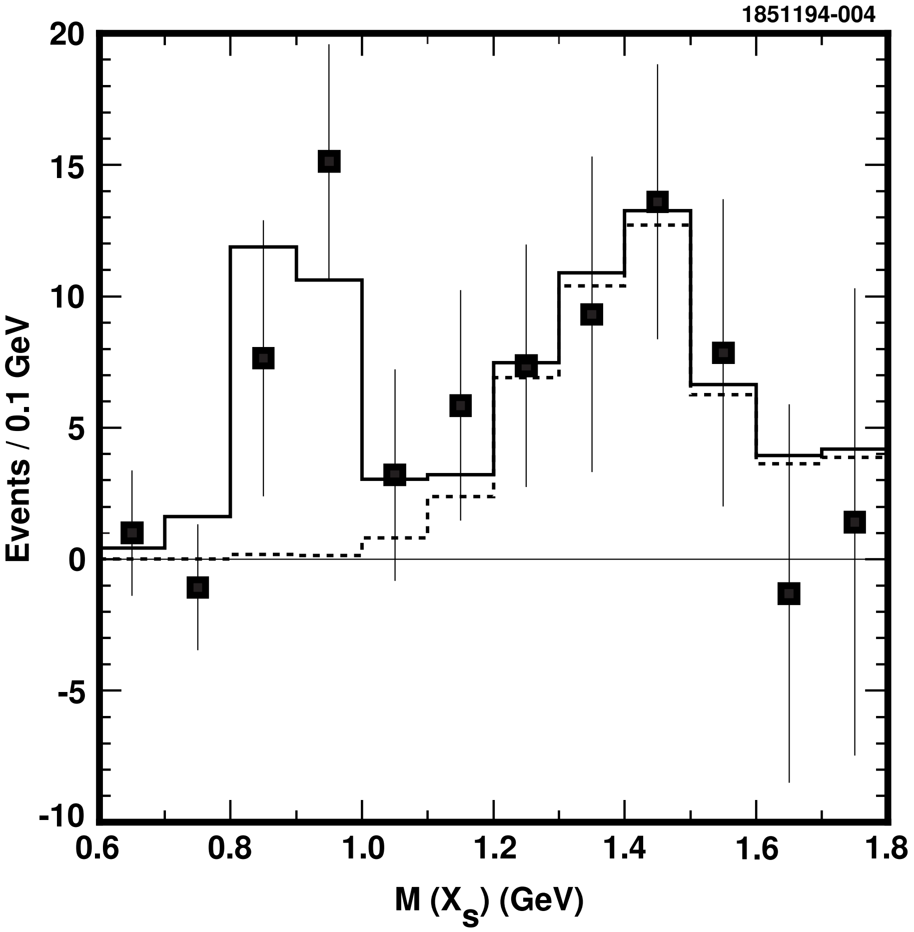

FIG. 4. Apparent X_s mass distribution from B-reconstruction analysis. Background-subtracted data, not corrected for efficiency or cross-feed (points); Monte Carlo fit, using several kaon resonances (solid histogram); component of fit from resonances other than $K^*(892)$ (dotted histogram).

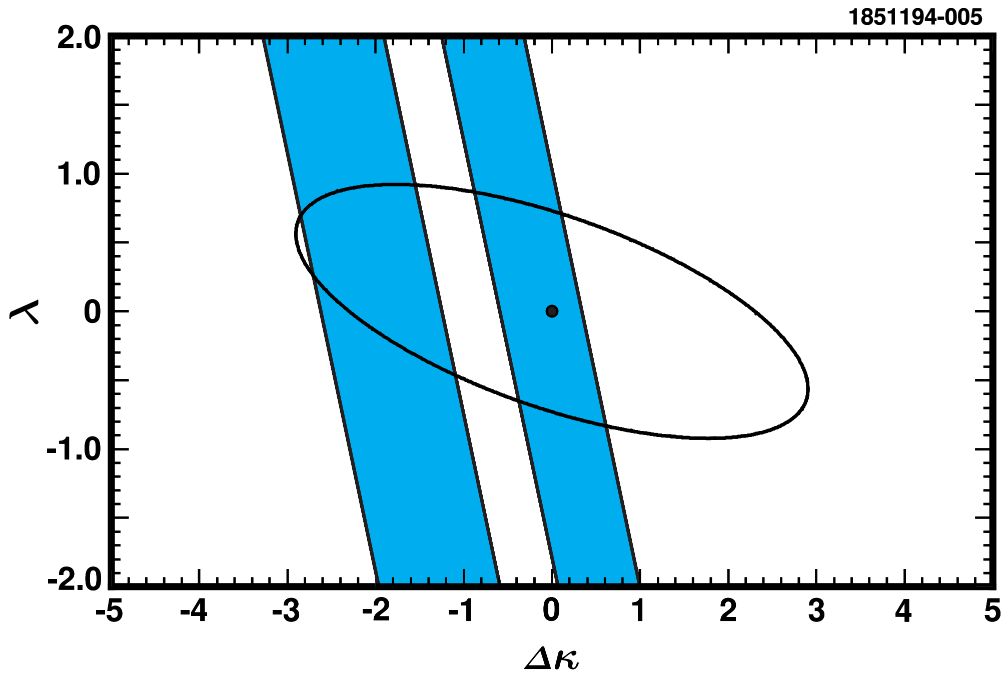

FIG. 5. Limits on anomalous $WW\gamma$ coupling parameters λ and $\Delta\kappa$. The shaded regions are consistent with the $b \to s\gamma$ branching ratio reported here. The region between the two shaded strips is excluded by the $b \to s\gamma$ lower limit, the outer unshaded regions by the upper limit. D0's yield of $p\bar{p} \to W\gamma X$ limits the allowed range to the interior of the ellipse (CDF obtains a similar ellipse)[19]. The Standard Model value is shown as the dot at $\Delta\kappa = \lambda = 0$.

TABLES

TABLE I. Yields of events with 2.2 - 2.7 GeV photons, for the two $b \to s\gamma$ analysis procedures.

	Event Shape	B Reconstruction
On	3013 ± 59	281 ± 17
Off(scaled)	2618 ± 73	155 ± 18
$\Upsilon(4S)$ background		
$b \to c$ MC	50.7 ± 5.1	12 ± 2
$b \to u$ MC	11.9 ± 4.0	2 ± 1
π^0 correction	50.2 ± 27.7	-0.7 ± 2.3
η correction	16.5 ± 33.7	2.0 ± 8.5
Non-$B\bar{B}$	2.3	
$\Upsilon(4S)$ total	132 ± 44	15 ± 9
On$-$Off$-\Upsilon(4S)$	263 ± 104	110 ± 26